Journal of
Manufacturing and Materials Processing

MDPI

Article

An Experimental and Numerical Study on Aluminum Alloy Tailor Heat Treated Blanks

Rui Pereira [1,*], Nuno Peixinho [1], Vítor Carneiro [1], Delfim Soares [1], Sara Cortez [1], Sérgio L. Costa [2] and Vítor Blanco [2]

[1] Mechanical Engineering Department (DEM), University of Minho, Campus de Azurém Av. da Universidade, 4800-058 Guimarães, Portugal
[2] Bairrimoldes Lda, Variante à EN 235 nº 33, 780-292 Anadia, Portugal
* Correspondence: a81833@alunos.uminho.pt

Abstract: Information is presented on the conceptualization, experimental study, and numerical process simulation of tailor heat treated aluminum alloy blanks. This concept is intended to improve the forming behavior of aluminum parts in challenging conditions. The implementation requires precise control of laser heat treatment parameters within a suitable industrial framework. The study details material properties, heat treatment parameters, and experimental results for the strength and elongation properties of an AA6063-T6 aluminum alloy. Constitutive modeling is applied using the Hocket–Sherby equation, which allowed us to establish a correlation between laser heat treatment maximum temperature and the corresponding material softening degree. Based on the generated flow stress–strain curves, a numerical simulation of a representative case study was performed with Abaqus finite element software highlighting potential improvements of tailor heat treated blanks (THTB). The influence and effectiveness of heat-affected zone (HAZ) dimensions and material softening were analyzed.

Keywords: AA6063-T6 aluminum alloy; forming; Hocket–Sherby equation; laser heat treatment; material softening; numerical simulation

Citation: Pereira, R.; Peixinho, N.; Carneiro, V.; Soares, D.; Cortez, S.; Costa, S.L.; Blanco, V. An Experimental and Numerical Study on Aluminum Alloy Tailor Heat Treated Blanks. *J. Manuf. Mater. Process.* **2023**, *7*, 16. https://doi.org/10.3390/jmmp7010016

Academic Editors: Chetan P. Nikhare and William J. Emblom

Received: 30 November 2022
Revised: 29 December 2022
Accepted: 30 December 2022
Published: 4 January 2023

1. Introduction

The automotive industry comprises an increasingly demanding and globalized sector. On one hand, the industry demands a competitive sector in which the reduction in production costs is the main concern. However, governmental legislation requires adequate responses from the manufacturing industries in order to deal with fuel emission levels [1,2]. In the quest to reduce the standards of greenhouse gas emissions, lightweight design manufacturing is at the forefront of research activities in the automotive industry [3,4]. Almost 40% of the vehicle is accounted for by the car body-in-white (BIW) structure [5]. As the sheet metal forming operation is the main manufacturing process used for BIW production [6], new and/or adapted technologies need to be developed to process the materials employed. Aluminum alloys are attractive materials to meet lightweight design and, therefore, have been employed [7]. However, such materials are characterized by low formability at ambient temperature [8,9], which may compromise the forming behavior and limit the geometrical complexity and dimensional control of manufactured components.

Several tools and techniques have been developed in order to overcome the low formability of aluminum alloys [10,11]. A possible approach is the implementation of tailored blanks concepts that are divided into four sub-groups: tailor welded blanks, patchwork blanks, tailor rolled blanks, and tailor heat treated blanks [12], see Figure 1. Tailor heat treated blanks (THTB) are characterized by local different mechanical properties which are optimized for the subsequent forming operation. The key idea is to locally heat treat previously identified blank zones which will allow the formation of a heterogeneous pattern of mechanical properties along the sheet metal. Mainly, the local heat treatment is performed

on the sheet surface before any forming operation [13]; nevertheless, the technology's effectiveness during multistage forming operations has also been demonstrated [14,15]. Geiger et al. [16] postulated that the local heat treatment should never be applied directly to the critical zones, but only to adjoining ones; otherwise, material failure and fractures would be more likely to occur.

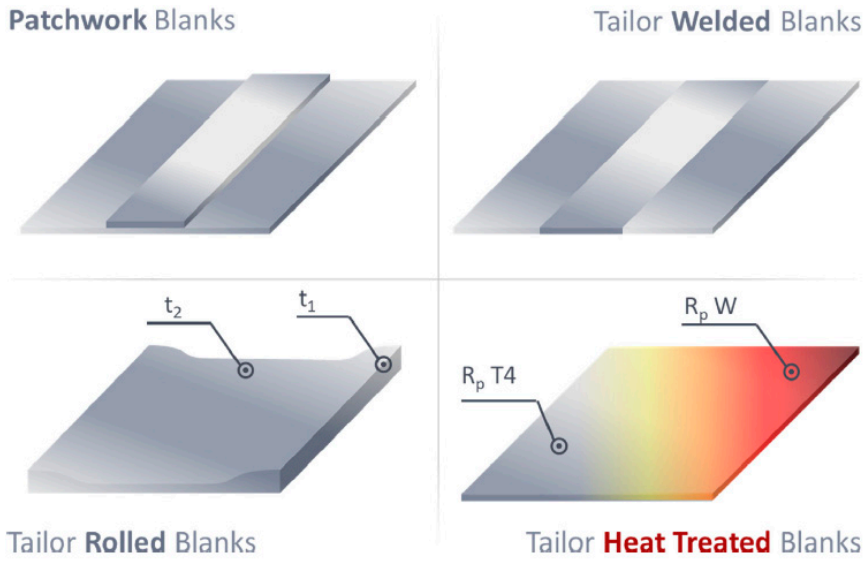

Figure 1. Classification of tailored blanks. Reprinted with permission from Ref. [12]. Copyright 2014, Elsevier.

Several heating technologies can be used to perform the local heat treatment such as laser radiation, electromagnetic induction, and heat conduction by heated contact plates. Due to its flexibility and the possibility of conducting the heat treatment layout at once, laser radiation is more commonly used [16]. Nevertheless, improved formability by adopting tailored heat treated blanks were also reported by means of using convective heating [17], particularly adequate for large heat-affected zones or by means of a specially developed contact heating tool [18].

The purpose of a THTB made out of precipitation hardenable materials, such as the 6xxx aluminum alloys, is to locally dissolve the *MgSi* clusters embedded in the aluminum matrix. The local microstructural modifications lead to material softening and mechanical resistance softening is observed, which can be accompanied by a ductility reduction [19]. The maximum temperature is mainly responsible for the activation of softening mechanisms; nevertheless, there is an underlying effect of the heating rate which cannot be neglected. On that account, differential scanning calorimetry (DSC) is a useful tool to investigate the kinematics of precipitation/dissolution reactions since it allows the establishment of a correlation between maximum temperature/heating rate with the activation of the microstructural mechanism. As noticed by the work developed by Osten et al. [20], higher heating rates shift dissolution/precipitation reactions toward higher temperatures, such as those obtained in a laser heat treatment.

The adapted specific pattern of soft and strength areas along the sheet metal enables both the material flow and local forces during the forming operation to be influenced. In order to investigate the forming behavior of tailor heat treated blanks, numerical simulation plays a key role in the optimization of the manufacturing process. The feasibility of the tailor heat treated blanks based on local heat treatment location and dimension has been investigated by numerical simulation. Geiger et al. [21] presented a numerical study on the influence of the local heat treatment layout, i.e., location and dimension. Their research concluded that a lower laser spot diameter, localized only in the peripheral zone of the blank, provides better drawing performance than a local heat treated layout in the force-transferring zone of the cup wall. Staud et al. [22] conducted an inverse approach

to determine the maximum temperature of local heat treatment which would provide the most effective formability enhancement of a cross-die geometry component. They reported that a drawing depth increase of 25 mm was possible. A similar approach was followed by Merklein et al. [23] to identify the most appropriate mechanical property distribution along the blank. Piccininni et al. [24] proposed an optimization loop for the determination of the parameters controlling the extension of the blank regions and the temperature distribution. Additionally, to define the optimum radial extension submitted to local heat treatment in order to maximize the limiting drawing ratio, an optimization platform was implemented [25].

2. Materials and Methods

2.1. Material Specifications

The material under investigation is a 6XXX aluminum alloy named 6063 in the artificially aged condition T6, with a sheet thickness of 2 mm. The base material's chemical composition is presented in Table 1. The specimens for purpose of the tensile tests size were selected based on limited material availability and were laser cut from an aluminum alloy 6063-T6. The specimen dimensions for uniaxial tensile tests are defined in Figure 2, which also highlights the HAZ.

Table 1. Chemical composition of the investigated alloy.

AA 6063-T6	*Al*	*Si*	*Ti*	*V*	*Mn*	*Fe*
	98.650	1.112	0.013	0.013	0.017	0.187

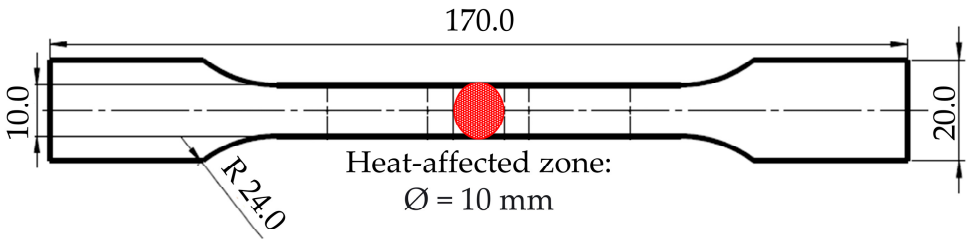

Figure 2. Heat-affected design and laser focus area.

2.2. Differential Scanning Calorimetry (DSC) Analysis

AA 6063-T6 precipitation sequence and phase change were studied by means of differential scanning calorimetry analysis prior to the laser heat treatment. This thermo-analytical technique is helpful in investigating the underlying effect of maximum temperature/heating rate on changes at the microstructural level, and hence on modification of the mechanical properties.

Figure 3a presents the equipment employed. The crucible is heated from room temperature up to 400 °C, while the heating rate is low enough to allow identification of precipitation/dissolution reactions. Pure aluminum is used as a reference material. The sample has a mass of 13 mg. The generated specific heat capacity curve plotted against the heating temperature is shown in Figure 3b allowing the detection of 2 precipitation reactions at 255 and 352 °C and 3 dissolution reactions at 203, 291, and 386 °C.

2.3. Local Laser Heat Treatment Equipment

The workpiece is submitted to the experimental procedure, i.e., to the local laser heat treatment using a 'Mergenthaler LM100' diode laser (Figure 4). In order to facilitate temperature uniformity and absorption along the heat-affected zone, a graphite coating named 'GRAPHIT 33' is applied. The process control is performed by a non-contact one-color pyrometer coaxially placed at the laser's head which measures the temperature on the surface directly exposed to laser radiation. Therefore, the laser equipment automatically adjusts laser power to meet the requested temperature. The process is characterized by no

movement of the laser beam. A cylindrical format for the focus region is used and the spot diameter always assumes the value of 10 mm.

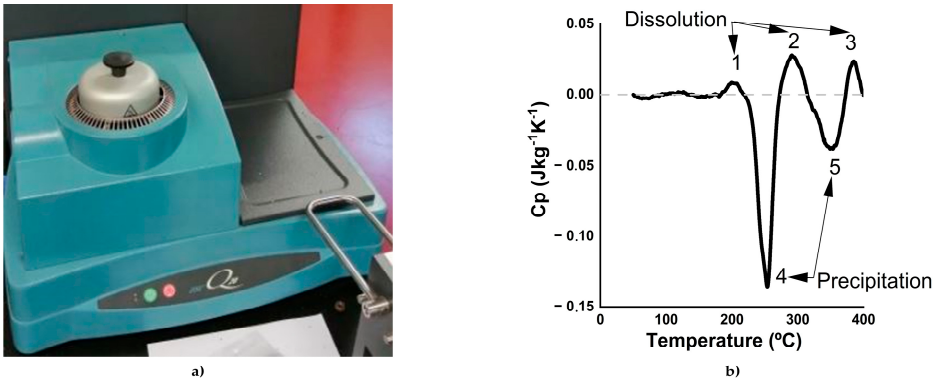

Figure 3. (**a**) 'DSC Q20' equipment used for calorimetry analysis. (**b**) Normalized specific heat capacity curve for a heating rate of 0.09 K/s.

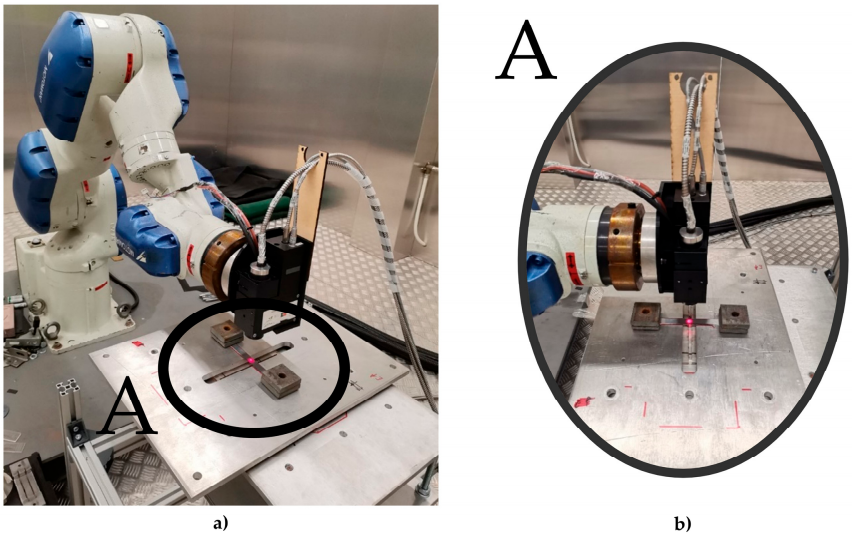

Figure 4. (**a**) 'LM100' diode laser head. (**b**) A detailed view of the specimen clamping fixture.

2.4. Finite Element Analysis of Deep Drawing Process Parametrization

The numerical simulation of a single-stage deep drawing process was performed with the standard implicit version of ABAQUS software (v. 2020).

The numerical analysis aims to demonstrate that the plastic-forming operation of tailored blanks with respect to material properties is improved by reducing the risk of fracture of the designed final component. Accordingly, a comparative analysis was carried out between the reference model, in which the base material mechanical properties are preserved throughout the entire blank, and several other models characterized by different degrees of mechanical resistance softening.

Thus, heat treated models' performance is investigated by the influence of two factors, these being (1) the heat treated region's location and dimension and (2) the mechanical resistance softening degree. In such a manner, it was possible to identify the appropriate minimum and maximum heat treated radial extension depending on the degree of softening imparted by the heat treatment at a selected maximum temperature. Table 2 contains the input variables range tested. A total of 80 hypotheses plus the reference model were simulated. The aim was to determine the most convenient set of parameters for deep drawing improvements.

Table 2. Input variables definition and delimitated range of corresponding values.

Input Variable	Variation Range															
Radial extension [mm] [1]	1	2	3	4	5	6	7	8	9	10	11	12	13	14	15	16
Target temperature [°C]		350				370				380				400				425	

[1] From the blank outer diameter (see Figure 5).

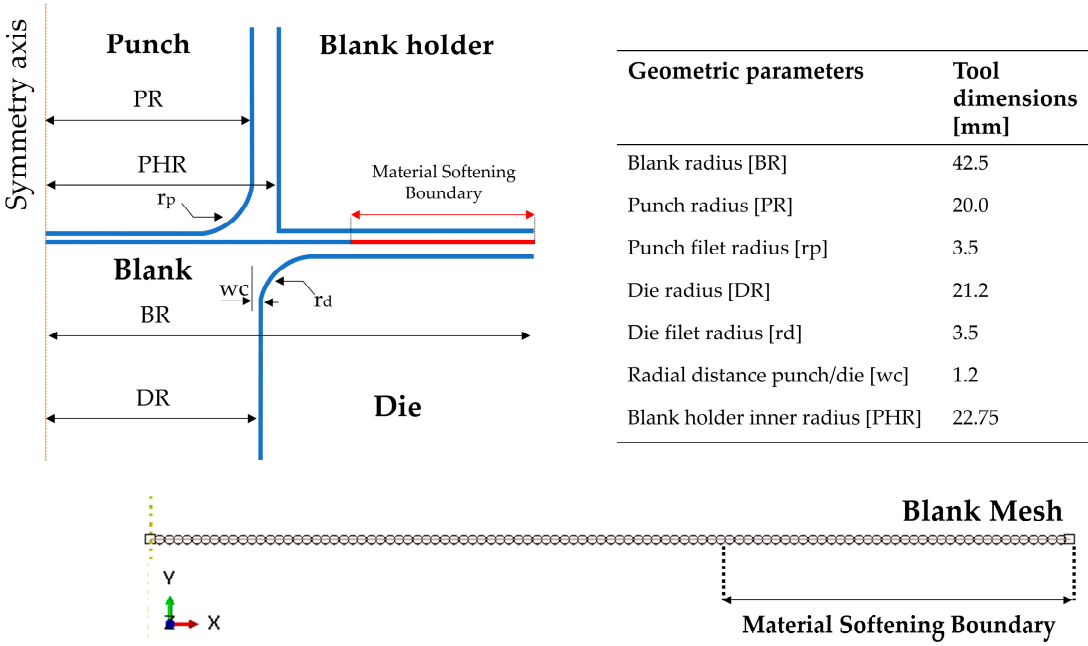

Geometric parameters	Tool dimensions [mm]
Blank radius [BR]	42.5
Punch radius [PR]	20.0
Punch filet radius [rp]	3.5
Die radius [DR]	21.2
Die filet radius [rd]	3.5
Radial distance punch/die [wc]	1.2
Blank holder inner radius [PHR]	22.75

Figure 5. Schematic representation of the 2D deep drawing process, including main dimensions and mesh characteristics.

The components' geometry and dimensions are shown in Figure 5. A 2D axisymmetric model was developed since it allows reduced computation time. As the scope of the analysis concerning the blank, the tools were modeled using analytical rigid surfaces. A vertical displacement of 30 mm is set to the punch. The step time is 1 s. A reduced gap between the blank and the blank holder was modeled. Therefore, during the simulation, the blank will come into contact at its top with the blank holder, which will remain in its original position whatever the force required to keep it fixed. The automatically calculated blank holder force varies during the process, achieving a maximum value of 12 kN. Meanwhile, the die remains in its original position. Regardless of the evaluated layout, the blank consists of a shell body with 100 elements of SAX1 type (2 nodes of a linear axisymmetric shell element). As noticed in Figure 5, the blank is modeled with two segments: a central zone with base material mechanical properties and an outside softened area with different mechanical properties. The penalty formulation was chosen to reproduce each of the contacts. The friction coefficient between punch and blank assumes the value of 0.16, while the pairs die/blank and blank holder/blank is 0.11. In addition, only half of the model was considered due to the geometry and material symmetry conditions.

With respect to the elastic behavior, it is assumed to be isotropic and described by a Poisson coefficient of 0.33 and a Young Modulus of 70 GPa, whereas the plastic behavior was modeled according to the stress–strain curves generated by Hocket–Sherby coefficients.

3. Results

3.1. Material Characterization

Softening mechanism activation is dependent on maximum temperature and heating rate. The goal is to select a maximum temperature at which dissolution reactions will occur.

Figure 6 presents the continuous heating dissolution diagram which allows the identification of dissolution/precipitation reactions at higher heating rates, such as those obtained in a laser application. The maximum temperature and heating rate of points B, C, and D in the figure allow these evaluated conditions to be located where a dissolution reaction takes place. Those were three of the four selected laser heat treatment maximum temperatures. Thus, it is expected that dissolution of β'' and GP-zones lead to material softening in this range of maximum temperatures. Point A is positioned where a precipitation reaction occurs. Details for creating this diagram are given by Osten et al. [20].

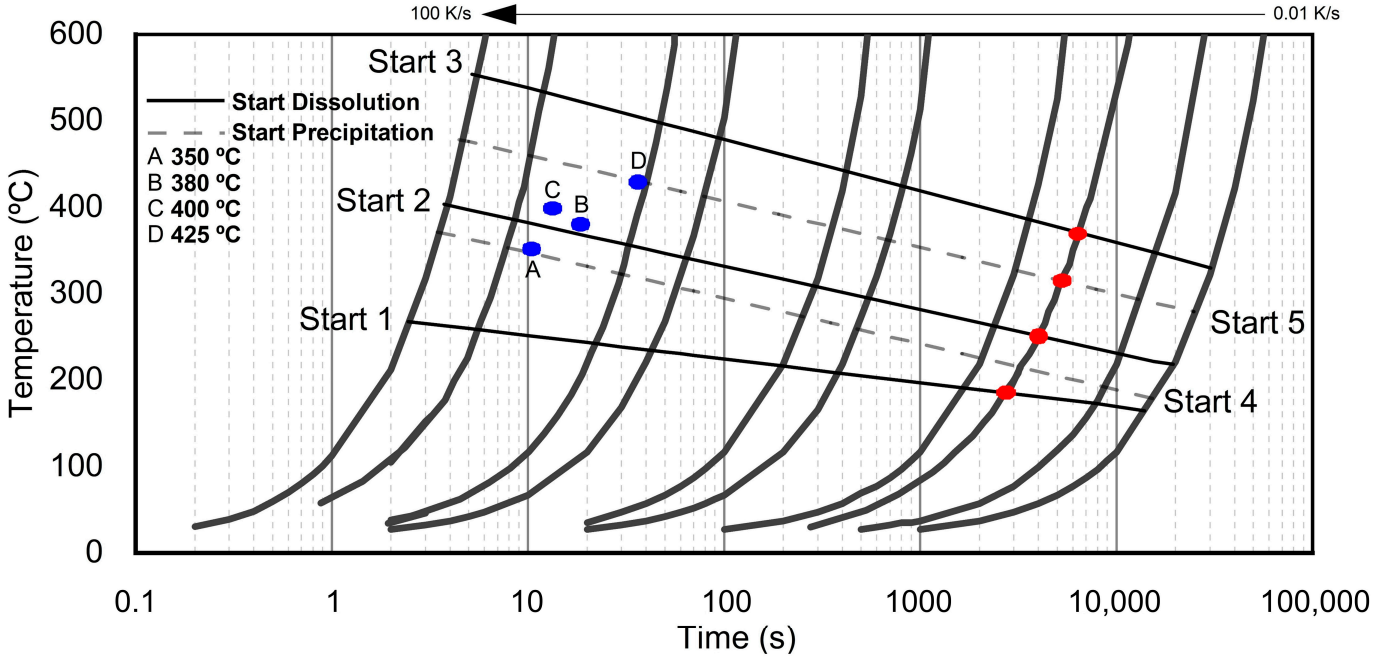

Figure 6. Localization of heat treatment maximum temperatures according to the predominant transformation phase in the continuous heating dissolution diagram.

Table 3 summarizes the correlation between heat treatment maximum temperature and the resulting mechanical properties modification for the evaluated laser heat treatment maximum temperatures. At 350 °C, material softening is barely noticeable; however, between 380 and 425 °C, a considerable mechanical resistance decrease is observed. The maximum degree of softening is achieved at a maximum temperature of 425 °C, corresponding to a yield stress and an ultimate tensile stress (UTS) decrease of 34 and 31%, respectively. Alongside material softening, ductility is negatively affected by the laser heat treatment, after laser heat treatment the strength increases again by natural aging [26]. The hardness measurements on both the incident surface and the opposite surface suggest that the heat treatment affected both surfaces almost equally.

Table 3. Mechanical property modification based on heat treatment maximum temperatures [19].

Nomenclature	Tmax [°C]	Hardness HV 30/20		Yield Stress [MPa]	UTS [MPa]	A60 [%]
		Incident Surf.	Opposite Surf.			
BM	Base Material	95		237.4	265.6	8.5
A	350	89	94	235.5	253.3	4.3
B	380	71	73	179.7	200.7	1.5
C	400	64	69	167.2	188.8	3.3
D	425	71	74	156.6	182.1	3.5

Figure 7 shows the fractured specimens of the four maximum laser heat treatment temperatures. The necking occurred in the heat treated area, i.e., in the central region of the specimens.

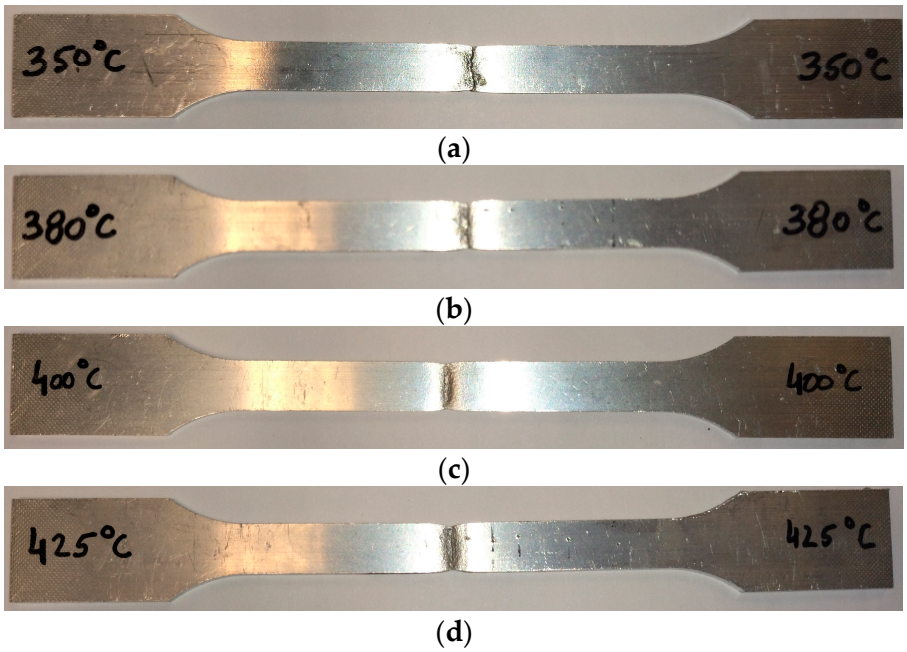

Figure 7. Fractured specimens by uniaxial tensile tests at a maximum laser heat treatment temperature of (**a**) 350 °C, (**b**) 380 °C, (**c**) 400 °C, and (**d**) 425 °C.

3.2. Derivation of a Temperature-Dependent Model

The application of the Hocket–Sherby constitutive model allowed the generation of stress–strain curves based on heat treatment maximum temperature. The model describes the strain-hardening behavior during plasticization with small increases at higher degrees of strain [27]. Equation (1) governs the Hocket–Sherby model, and it was applied for an AA6063-T6 aluminum alloy, where φ represents the plastic strain.

The curve describing the strain hardening starts with the initial yield stress expressed by coefficient A. Meanwhile, tensile stress is represented by coefficient B. These two parameters were determined based on four laser heat treatment maximum temperatures: $T_{max} = 350, 380, 400,$ and 425 °C. The material hardening is depicted by both coefficients C and D. Thus, the coefficients of the Hocket–Sherby equation are expressed as a function of maximum heat treatment temperature (Table 4).

$$\sigma(\varphi) = B - (B - A) \times e^{(-C \times \varphi^D)} \quad (1)$$

Table 4. Equations of Hocket–Sherby coefficients as a function of maximum temperatures for AA6063-T6.

Material	Coefficient Equations
AA 6063-T6	$A = 0.0174T_{max}^2 - 14.53T_{max} + 3156.1$ $B = 0.0182T_{max}^2 - 15.129T_{max} + 3321.2$ $C = 0.0737T_{max} - 12.474$ $D = 0.51$

In order to verify the validity of the maximum temperature-dependent material derivation model, the experimental curve recorded in tensile tests at a maximum temperature of 400 °C was compared with the value obtained by the Hocket–Sherby model. As shown in Figure 8a, the coefficient reliably reflects the trend of the respective experimental curve. The maximum error for the recorded stress values between both curves is 5%.

Figure 8b summarizes generated flow curves for maximum temperatures at the range of $350 < T_{max} < 425$ °C. AA6063-T6 material characterization by applying the Hocket–Sherby coefficient as a function of heat treatment maximum temperature provides useful information for in-data numerical simulation in order to optimize the maximum temperatures of interest in a sheet metal plastic forming process made of THTB.

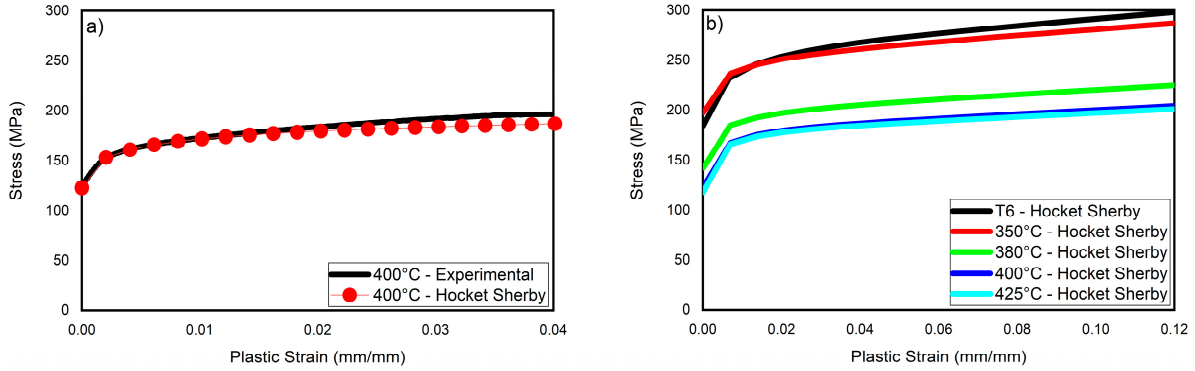

Figure 8. Stress–strain curves. (**a**) A comparison of the experimental and the generated curve by the Hocket–Sherby model and (**b**) the generated Hocket–Sherby curves at different conditions.

3.3. Deep Drawing of Numerical Tailored Blanks

The influence of both the heat-affected zone dimension and mechanical resistance softening are investigated by means of (1) punch force required to deform the blank; (2) sheet thickness evolution along blank radial extension; and (3) strain distribution. This output provides useful information regarding the forming behavior. The results show that both the heat-affected zone dimension and material softening degree affects cup performance.

Figure 9 compares the numerical evolution of the punch force and displacement. In Figure 9a, the influence of the heat-affected zone dimension is analyzed, while in Figure 9b, the influence of the degree of softening of the material is investigated.

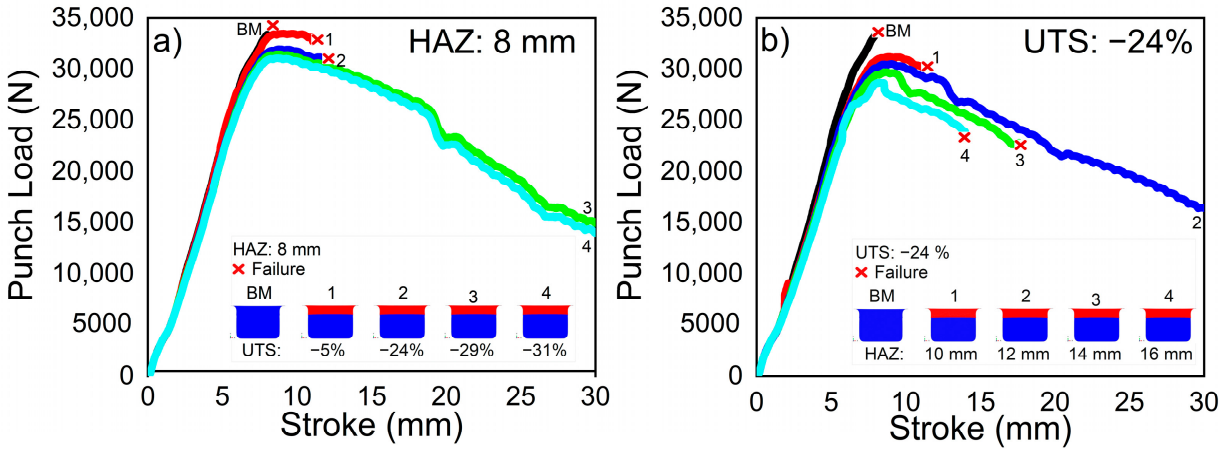

Figure 9. Punch load and punch displacement of the reference model and several heat treatment conditions. (**a**) Varying material softening degree and (**b**) modifying the heat-affected zone dimension.

The maximum drawing depth of the reference material is low, at about 9 mm. Additionally, the higher the mechanical resistance softening, the more likely the component is to be successfully produced. While for an ultimate tensile stress decrease of 5%, the component fractures are at a punch displacement of 10 mm and a successfully produced cup is possible for material softening of 29 and 31% (Figure 9b). Therefore, using a HAZ

not close to the component's critical zone means that the material softening needs to be high for significant improvements in the forming behavior.

A material softening corresponding to a UTS decrease of 24% on the influence of the heat-affected zone dimension is observed in Figure 9b. All models reveal improved forming behavior in comparison to the reference model. In fact, the cup is produced without failure for a heat-affected zone of 12 mm, corresponding to an ultimate tensile stress decrease of 24%. However, the closer the heat-affected zone is to the critical zone, the lower the drawing depth.

The higher the heat-affected zone and/or the material softening, the lower the maximum punch load: −9% for a HAZ of 12 mm and a maximum temperature of 425 °C. Therefore, the energy costs associated with the forming process may be lower.

Figure 10 presents a graphical comparison of the sheet thickness between the base material model at a punch displacement of 9 mm with laser heat-treated models, characterized by a heat-affected zone of 8 mm and several degrees of ultimate tensile stress decrease, at a drawing depth of 30 mm. For the reference model as well as model 1 (ΔUTS = −5%) and 2 (ΔUTS = −24%), fractures occur in the critical zone. A substantial reduction of 68% compared to the initial sheet thickness is observed for a punch displacement of only 9 mm for the base material model. On the other hand, higher laser heat treatment maximum temperatures corresponding to a more significant ultimate tensile stress decrease allows cup production without failure. A maximum reduction of 20% in the sheet thickness is noticed. In the peripheral zone of the blank, the thickness exceeds its initial value, possibly due to the effect of material flow; the material has dislocated from the center to the outer region.

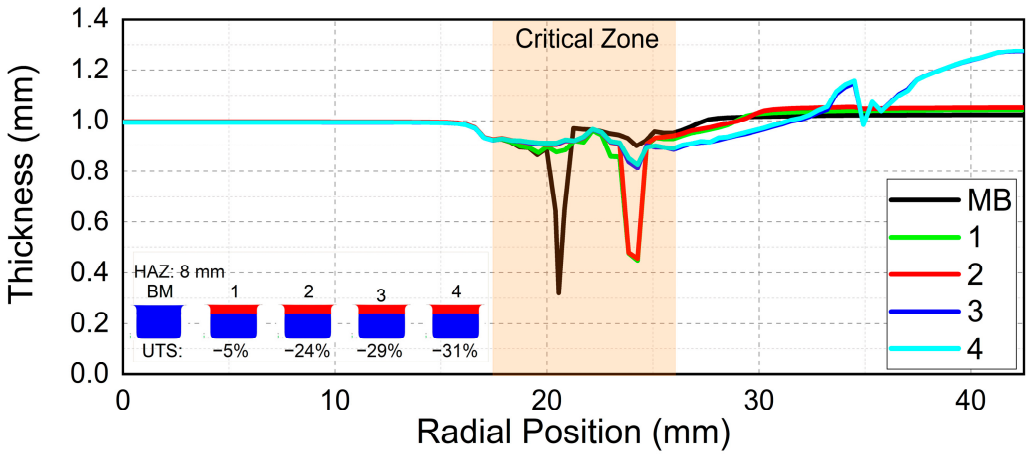

Figure 10. Comparison of component final thickness evolution along radial extension for different degrees of material softening with a HAZ of 8 mm.

The final sheet thickness distribution along the cup's wall is depicted in Figure 11 for the reference model and a heat treated layout. As can be observed, failure occurs in the corner area when the conventional blank is formed. On the contrary, results show the possibility of a 30 mm drawing depth for the heat treated model, representing a reduction of less than 20% of the initial sheet thickness.

Figure 12 compares the strain distribution obtained for the surface of the cup at a drawing depth of 9 mm and 30 mm for the base material model and a tailor heat treated model (HAZ = 12 mm and ΔUTS = −29%), respectively. Some strains measured at Zone 2 and 3 present values higher than the FLC curve. However, it does not mean that the piece will crack. Therefore, all the strains below the FLC curve are in a safe zone, while for strains above, localized necking occurs which potentially may lead to material rupture. Additionally, both models in Zone 4 have high values of minor strain which indicate a tendency for wrinkling.

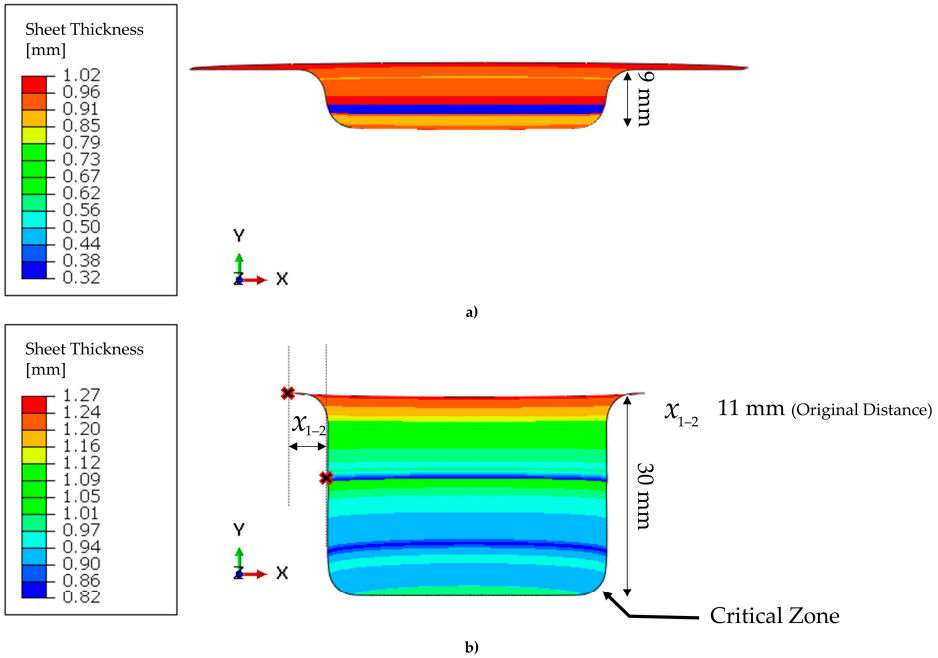

Figure 11. Final sheet thickness distribution along the cup's wall for (**a**) the base material model and (**b**) the heat treated model. HAZ = 11 mm and ΔUTS = 29%.

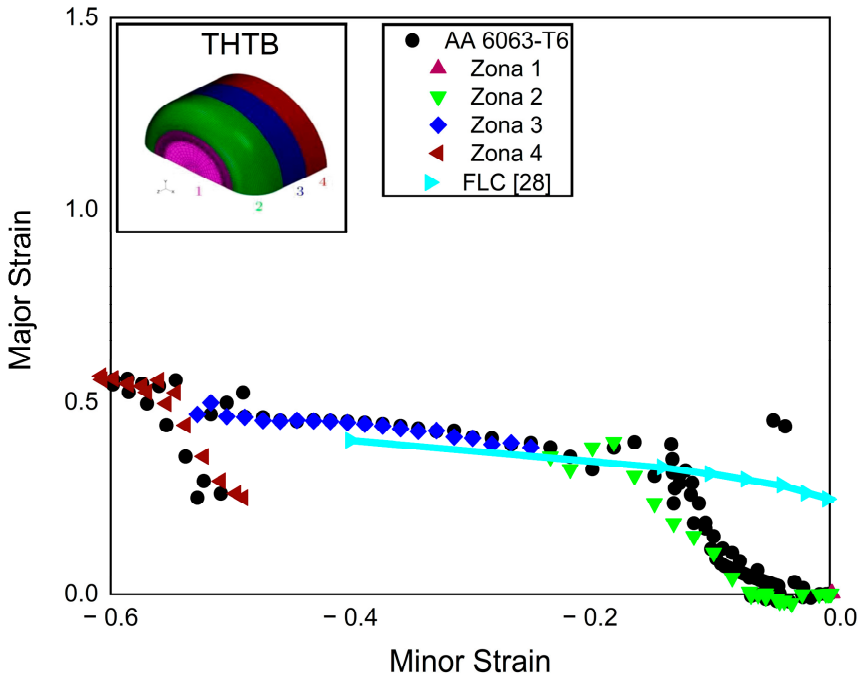

Figure 12. Strain distribution and forming the limit diagram of THTB and conventional AA6063-T6 at a punch displacement of 30 mm and 9 mm, respectively. We added an extrapolated point from the original reference [28] at a minor strain value of 0.4.

Although forming behavior of both models evaluated in this figure seems similar, the two black dots at the top-right corner are evidence that failure appears in the conventional blank. Regarding the THTB model, although the model steps into the limit of rupture, the major strain values in the punch radius (Zone 2) are significantly lower since they is not observed as a clear deviation from the FLC curve. The strain distribution in the critical corner can be shortened. The forming capacity of the corner radius of the tailored blank is

improved when compared to the base material strain distribution at a substantially lower drawing depth (9 mm).

4. Discussion

Material softening in terms of yield and ultimate tensile strength decrease is successfully achieved at the maximum temperature range of 380–425 °C. The modified mechanical properties are caused by the dissolution of β'' and GP Zones. Material characterization based on heat treatment maximum temperature provided useful information for in-data numerical simulation.

The deep-drawn base material model fractures at an early stage of the punch displacement. As the load applications start, the blank is bent onto the round edge of the die cavity. With further increase in the load, the component is straightened. However, as the material flow is insufficient, component failure occurs. This occurs for 44% of the evaluated heat treated layouts, independently of the HAZ dimension and material softening degree, as observed in Figure 13, which compiles all the evaluated models.

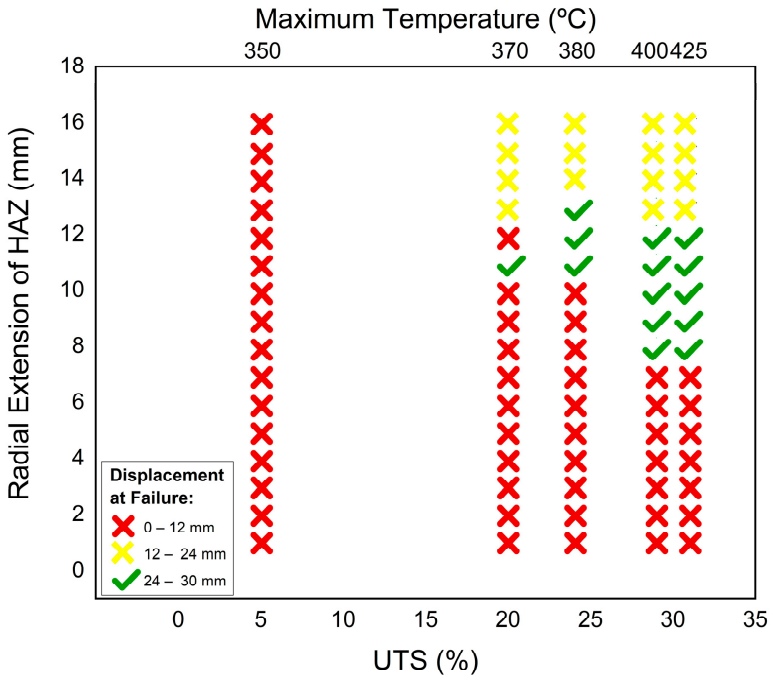

Figure 13. Compilation of all evaluated THTB simulated models and qualification of drawing depth based on material softening degree and HAZ dimension.

However, the higher the HAZ adjacent to the critical zone, the easier the material flow and hence, the higher the drawing depth. Furthermore, the higher the material softening, the more probabilities there are of a successful cup production, as shown in Figure 13 and Table 5.

Table 5. Material softening degree and heat-affected zone dimension upper and minimal values to meet a successfully produced component at a punch displacement of 30 mm.

Tmax [°C]	UTS Reduction [%]	Heat-Affected Zone Dimensions [mm]	
		Upper Bound [mm]	Minimal Bound [mm]
350	−5	-	
370	−20	11	11
380	−24	11	13
400	−29	8	12
425	−31	8	12

Furthermore, a minimum of an 8 mm laser heat treated region or an ultimate tensile stress decrease of 20% are necessary so that the component can be successfully produced, otherwise tailored blank improvement is barely noticeable. Additionally, the higher the material softening, the smaller the heat-affected zone dimension needed.

5. Conclusions

In the present work, AA6063-T6 material softening due to a local laser heat treatment is correlated with heat treatment maximum temperature, as well as the heating rate. DSC calorimetry analysis shows that the dichotomy heating rate/maximum temperature is important for the occurrence of dissolution reactions leading to material softening.

The application of tailor heat treated blanks leads to improvements in the forming behavior of aluminum alloy components, as demonstrated in the literature. The present work aims at evaluating the influence of heat-affected zone dimension and material softening degree, i.e., maximum heat treatment temperature in the drawing depth of a circular cup. The simultaneous analysis of these two parameters allowed us to establish that the heat-affected zone dimension can be shortened if a higher material softening degree is imparted by a higher maximum laser heat treatment temperature. Conversely, a higher heat-affected zone is required in the case of a lower material softening degree. Therefore, based on tool parameters and blank dimensions, the optimal combination between the heat treatment dimension and the heat treatment maximum temperature should be achieved.

Author Contributions: Conceptualization, R.P., N.P. and S.L.C.; Data curation, R.P., N.P., V.C. and S.L.C.; Formal analysis, R.P., N.P. and S.L.C.; Funding acquisition, N.P., S.L.C. and V.B.; Investigation, R.P. and N.P.; Methodology, R.P., N.P., D.S. and S.L.C.; Project administration, S.C., S.L.C. and V.B.; Resources, V.C.; Software, V.C. and D.S.; Supervision, N.P. and S.L.C.; Validation, S.C., S.L.C. and V.B.; Visualization, R.P. and N.P.; Writing—original draft, R.P., N.P. and V.C.; Writing—review and editing, R.P., N.P., D.S., S.C., S.L.C. and V.B. All authors have read and agreed to the published version of the manuscript.

Funding: This research was funded by Projects I&DT SIT—Softening in Tool, grant number CENTRO-02-0853-FEDER-045419 and METRICS (UID/EMS/04077/2020).

Institutional Review Board Statement: Not applicable.

Data Availability Statement: Not applicable.

Conflicts of Interest: The authors declare no conflict of interest.

References

1. Fang, H.; Jiang, C.; Hussain, T.; Zhang, X.; Huo, Q. Input digitization of the manufacturing industry and carbon emission intensity based on testing the world and developing countries. *Int. J. Environ. Res. Public Health* **2022**, *19*, 12855. [CrossRef] [PubMed]
2. Hirsch, J. Aluminium in innovative light-weight car design. *Mater. Trans.* **2011**, *52*, 818–824. [CrossRef]
3. Tisza, M.; Czinege, I. Comparative study of the application of steels and aluminium in lightweight production of automotive parts. *Int. J. Lightweight Mater. Manuf.* **2018**, *1*, 229–238. [CrossRef]
4. Czerwinski, F. Current trends in automotive lightweighting strategies and materials. *Materials* **2021**, *14*, 6631. [CrossRef] [PubMed]
5. Dama, K.K.; Babu, V.S.; Rao, R.N. State of the art on automotive lightweight body-in-white design. *Mater. Today Proc.* **2018**, *5*, 20966–20971. [CrossRef]
6. Kumar, K.P.; Kumar, K.M.; Sudhakar, U. Design for manufacturability of automotive part considering formability and springback. *Int. J. Mech. Eng.* **2014**, *3*, 45–52.
7. Andersson, O.; Semere, D.; Melander, A.; Arvidsson, M.; Lindberg, B. Digitalization of process planning of spot welding in body-in-white. *Procedia CIRP* **2016**, *50*, 618–623. [CrossRef]
8. Schneider, R.; Heine, E.; Grant, R.J.; Zouaoui, Z. Aluminium sheet metal forming at low temperatures. *IOP Conf. Ser. Mater. Sci. Eng.* **2015**, *74*, 012014. [CrossRef]
9. Ismail, A.; Mohamed, S.M. Review on sheet metal forming process of aluminium alloys. In Proceedings of the 17th AMME Confernce, Cairo, Egypt, 19–21 April 2016.
10. Muwei, S. Methods to improve the performance of aluminum alloy. *IOP Conf. Ser. Earth Environ. Sci.* **2021**, *783*, 012053.
11. Zheng, K.; Politis, J.D.; Wang, L.; Lin, J. A review on forming techniques for manufacturing lightweight complex—Shaped aluminium panel components. *Int. J. Lightweight Mater.* **2018**, *1*, 55–80. [CrossRef]

12. Merklein, M.; Johannes, M.; Lechner, M.; Kuppert, A. A review on tailored blanks- production, applications and evaluation. *J. Mater. Process. Technol.* **2014**, *214*, 151–164. [CrossRef]
13. Nguyen, H.; Merklein, M. Improved formability of aluminum alloys using laser induced hardening of tailored heat treated blanks. *Phys. Procedia* **2012**, *39*, 318–326.
14. Merklein, M.; Bohm, W.; Lechner, M. Tailoring material properties of aluminum by local laser heat treatment. *Phys. Procedia* **2012**, *39*, 232–239. [CrossRef]
15. Lechner, M.; Johannes, M.; Kuppert, A.; Merklein, M. Influence of pre-straining and heat treatment on the yield surface of precipitation hardenable aluminum alloys. *Phys. Procedia* **2014**, *56*, 1400–1409. [CrossRef]
16. Geiger, M.; Merklein, M.; Vogt, U. Aluminum tailor heat treated blanks. *Prod. Eng. Res. Dev.* **2009**, *3*, 401–410. [CrossRef]
17. Kahrimanidis, A.; Lechner, M.; Degner, J.; Wortberg, D.; Merklein, M. Process design of aluminum tailor heat treated blanks. *Materials* **2015**, *8*, 8524–8538. [CrossRef]
18. Machhammer, M.; Sommitsch, C. The interaction between short-term heat-treatment and the formability of an Al-Mg-Si alloy regarding deep drawing processes. *IOP Conf. Ser. Mater. Sci. Eng.* **2016**, *159*, 012001. [CrossRef]
19. Peixinho, N.; Pereira, R.; Carneiro, V.; Costa, S.; Blanco, V. Development of laser heat treatment process for assisted forming of aluminum alloys. In Proceedings of the 2021 6th International Conference Smart Sustainability Technology SpliT, Split, Croatia, 8–11 September 2021.
20. Osten, J.; Milkereit, B.; Schick, C.; Kessler, O. Dissolution and precipitation behaviour during continuous heating of Al-Mg-Si alloys in a wide range of heating rates. *Materials* **2015**, *8*, 2830–2848. [CrossRef]
21. Geiger, M.; Merklein, M.; Kerausch, M. Finite element simulation of deep drawing of tailored heat treated blanks. *CIRP Ann. Manuf. Technol.* **2004**, *53*, 223–226. [CrossRef]
22. Staud, D.; Merklein, M. Inverse approach to the forming simulation of tailor heat treated blanks. *Int. J. Mater. Form.* **2008**, *1*, 37–40. [CrossRef]
23. Merklein, M.; Geiger, M.; Staud, D.; Vogt, U. Tailored heat treated blanks applied on car body parts under quasi-series conditions. *Int. J. Microstruct. Mater. Prop.* **2009**, *4*, 525–533. [CrossRef]
24. Piccininni, A.; Di Michele, G.; Palumbo, G.; Sorgente, D.; Tricarico, L. Improving the hydromechanical deep-drawing process using aluminum tailored heat treated blanks. *Acta Metall. Sin-Engl.* **2015**, *28*, 12. [CrossRef]
25. Piccininni, A.; Palumbo, G. Design and optimization of the local laser treatment to improve the formability of age hardenable aluminium alloys. *Materials* **2020**, *13*, 1567. [CrossRef] [PubMed]
26. Fröck, H.; Graser, M.; Milkereit, B.; Reich, M. Precipitation behaviour and mechanical properties during short-term heat treatment of tailor heat treated profiles (THTP) of aluminum alloy 6060 t4. In *Materials Science Forum*; Trans Tech Publications Ltd.: Wollerau, Switzerland, 2016; Volume 877, pp. 400–406.
27. Vogt, U. Seriennahe Auslegung Von Aluminium Tailored Heat Treated Blanks. Ph.D. Thesis, Technischen Fakultat der Friedrich-Alexander-Universitat Erlangen-Nurnberg, Erlangen, Germany, 2009.
28. Prillhofer, R.; Rank, G.; Berneder, J.; Antrekowitsch, H.; Uggowitzer, J.P.; Pogatscher, S. Property criteria for automotive Al-Mg-Si sheet alloys. *Materials* **2014**, *7*, 5047–5068. [CrossRef]